

Iron Recovery from Iron Ore Tailings by Direct Hydrogen Reduction at Low Temperature and Magnetic Separation

Paula S. Pinto,¹ *^{a,b} Luisa E. Milagre,^a Larissa C. M. Moreira,^a Hamilton P. Rocha Junior,^a Adriana B. Salviano,^a José D. Ardisson,^c Fabrício V. Parreira,^d Ana Paula C. Teixeira^a and Rochel M. Lago¹ ^a

^aDepartamento de Química, Universidade Federal de Minas Gerais (UFMG),
31270-901 Belo Horizonte-MG, Brazil

^bGrupo de Materiais e Tecnologias Ambientais, Universidade do Estado de Minas Gerais (UEMG),
Campus Divinópolis, 35501-170 Divinópolis-MG, Brazil

^cLaboratório de Física Aplicada, Centro de Desenvolvimento da Tecnologia Nuclear, CDTN/CNEN,
31270-901 Belo Horizonte-MG, Brazil

^dCentro de Tecnologia de Ferrosos, Vale S.A., 34000-000 Nova Lima-MG, Brazil

In this work, we describe a sustainable alternative to recover iron from two iron ore tailings (IOT) using hydrogen reduction at relatively low temperatures followed by magnetic separation. X-ray powder diffraction (XRD), inductively coupled plasma (ICP), atomic absorption (AA), Mössbauer, scanning electron microscopy (SEM/EDS), Raman and thermogravimetry (TG) analyses indicated that the Fe oxide present in the IOTs (sandy tailing (ST) and mud tailings (MT)), can be reduced with H₂ at 500 °C to produce α -Fe. Upon magnetic separation the mud tailing produced a 77 wt.% magnetic fraction increasing the Fe content from 19.2 to ca. 56 wt.% of Fe. On the other hand, the sandy tailing resulted in a 15 wt.% magnetic fraction increasing the Fe content from 19.2 to 70 wt.%. These results indicate that up to 86% of iron can be recovered from the IOT wastes already in the metallic form which can be very interesting for the steel industry.

Keywords: hydrogen, iron ore tailing, iron, magnetic separation, recovery, reduction



Introduction

Brazil is the second largest iron ore producer in the world with an estimated production of 400 million tons of iron ore in 2020.¹ During iron ore processing and beneficiation, two types of iron ore tailings (IOT) are produced, sandy and mud tailings. The comminuting process generates fine particles, due to rough crushing and fine grinding, and a desliming process is needed. In this step, fine particles are removed and the mud tailing is generated. It is generally composed of fine aggregated particles rich in iron oxides mainly hematite (α -Fe₂O₃) and goetite (α -FeOOH) and a fraction of quartz (SiO₂). The step after comminuting is flotation, where iron oxide particles are segregated from quartz. Another iron ore waste generated is the sandy tailing, which is

constituted mainly of quartz and small fractions of iron oxide.² Besides the iron oxides and silica, the IOTs have small amounts of aluminum, calcium and magnesium phases.³⁻⁵

The generation of iron ore tailings depends on the beneficiation process. The generation of iron ore tailings in Brazil is estimated at 20-40% by the weight of the total iron ore mining.^{6,7} In 2017, 562 million tons of mining tailings were produced just in the state of Minas Gerais (Brazil).⁸ Several environmental problems have been associated to the iron ore tailings (IOTs), such as pollution of ground and surface water^{9,10} and disposal dams, causing serious environmental accidents, such as the collapses of the Fundão (Mariana, Brazil, 2015) and Mina do Feijão dams (Brumadinho, Brazil, 2019).

Numerous studies have been conducted in order to find some application for IOTs. They have been used to produce building materials,^{11,12} geopolymers,^{13,14} in the synthesis of mesoporous silica,¹⁵ as catalyst for the

*e-mail: paula.sevenini@uemg.br

Editor handled this article: Luiz Ramos (Guest)

growth of carbon nanotube,¹⁶ oxidation of formaldehyde,¹⁷ oxidation of contaminants^{18,19} and as adsorbent of metals¹³ and dyes.²⁰

Several works have found IOTs with varying amounts of iron, from ca. 6 to 50 wt.%.⁶ Considering that 1.4 billion tons of iron ore tailing wastes (IOT) are generated *per* year all over the world²⁰ and the lowest amount of iron (6 wt.%), this means that 84 millions of tons of metallic iron will be wasted. Moreover, the high-grade iron ore deposits are becoming scarcer due to continuous depletion of mineral resources. Then, it is interesting and strategic the recovery of iron from the iron ore tailings, especially using clean and environmentally friendly processes. Flotation and roast reduction/magnetic separation are the main processes investigated to recover iron from the tailings.²¹ Although, flotation is a widely used process in the mining industry, limited efficiencies have been obtained mainly due to granulometry of the tailings.^{22,23} The roast reduction followed by magnetic separation consists in the use of coal or CO to produce magnetic iron phases, mainly magnetite, at temperatures usually higher than 530 °C.^{3,5,24,25}

The reduction of iron ore tailing with H₂ is a cleaner and environmental friendly process, that can replace coke and eliminate the generation of the greenhouse gases CO and CO₂.²⁶ The direct reduction of iron oxides using hydrogen is far reported for synthetic iron oxides^{27,28} and iron ores.²⁹⁻³¹ However, most of those studies obtained metallic iron at high temperatures (ca. 700-1000 °C) and there is a lack of information about the use of hydrogen at relatively low temperatures to recover iron in metallic form from iron ore tailings.

In this work, we describe the use of hydrogen at low temperature (500 °C) in order to produce and separate metallic iron from two iron ore tailings, sandy and mud.

Experimental

The two iron ore tailings (ST = sandy tailing, MT = mud tailing), with different iron content (wt.%) were initially dried at 120 °C for 24 h.

The iron tailings were direct reduced by heating 500 mg at 10 °C min⁻¹ up to 500 °C in a tubular furnace and holding for 3 h with pure H₂ (50 mL min⁻¹, Air Products, Mogi das Cruzes-SP, Brazil). The obtained materials were named as ST_{Rd}500 and MT_{Rd}500.

The magnetic separation was carried out initially dispersing 50 mg of the material in distilled water and ultrasound during 15 min. Then, using a neodymium magnet, the wet mixture was separated into two fractions, magnetic (MF) and nonmagnetic (NMF). After this procedure, the fractions were dried at 200 °C overnight.

The physicochemical properties of the iron tailings, before and after reduction treatment and magnetic separation, were analyzed by different techniques.

In order to investigate the different phases presented on iron tailings and in which they had been transformed after reduction and magnetic separation, inductively coupled plasma (ICP Varian 715 ES, Agilent, Melbourne, Australia), X-ray powder diffraction (XRD, Shimadzu XRD-7000 Cu radiation, 4° min⁻¹, Osaka, Japan), Mössbauer spectroscopy (⁵⁷Co source in a Rh matrix using α -Fe as reference spectrum at room temperature, Wissenschaftliche Elektronik GmbH, Starnberg, Germany), and Raman spectroscopy (SENTERRA, Bruker, 633 nm, 0.2 mW laser, Ettlingen, Germany) were carried out. The interpretation of the observed reflections in XRD was made using the database of the Crystallographica Search-Match software.

The particle morphology was studied by scanning electron microscopy (SEM, Quanta 200 FEI and Quanta FEG 3D FEI microscopes, FEI/Thermo Fischer Scientific, Eindhoven, Netherlands). Simultaneously, energy dispersion X-ray spectroscopy (EDS) was performed to obtain the chemical distribution of elements, as iron and silicon. The generated images by SEM were treated, when necessary, in the ImageJ software.³²

Thermogravimetric analysis (TG/DTG, Shimadzu-60H, performed in air atmosphere with a heating rate of 10 °C min⁻¹ up to 900 °C, Osaka, Japan), atomic absorption (AA, VARIANA A240FS with flame atomizer, Melbourne, Australia), were used to further understand the chemical composition and thermal modification of materials.

Results and Discussion

Direct reduction

In this work it was used two tailings from iron ore processing, i.e., a very fine Fe oxide rich mud waste (named hereon MT-mud tailing) and a silica rich waste similar to a sand named hereon as sandy tailing (ST). These tailings were characterized by inductively coupled plasma (ICP), powder X-ray diffraction (XRD), Mössbauer spectroscopy, scanning electron microscopy (SEM) and Raman spectroscopy.

The chemical composition of the samples was obtained by ICP analyses and indicated the presence of 19.2 wt.% of elemental Fe (which corresponds to 27% of Fe₂O₃) and 71 wt.% of SiO₂ for the sandy tailing sample (ST). On the other hand, the mud tailing (MT) showed ca. 50.2 wt.% of elemental Fe (which corresponds to 71% of Fe₂O₃) and 14 wt.% of SiO₂. Other elements were found but at lower

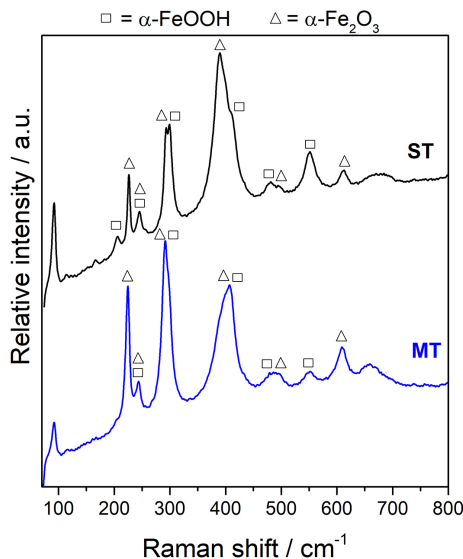
Table 1. Chemical composition of ST and MT obtained by XRF analyses

Sample	Fe / wt.%	SiO ₂ / wt.%	Al ₂ O ₃ / wt.%	P / wt.%	Mn / wt.%	CaO / wt.%	MgO / wt.%	TiO ₂ / wt.%
ST	19.2	70.8	0.61	0.022	0.014	0.013	0.024	0.033
MT	50.2	14.1	5.64	0.137	0.156	0.100	0.094	0.227

ST: sandy tailing; MT: mud tailing.

levels, such as Al (as Al₂O₃), Ti (as TiO₂) and Ca (as CaO) (Table 1).

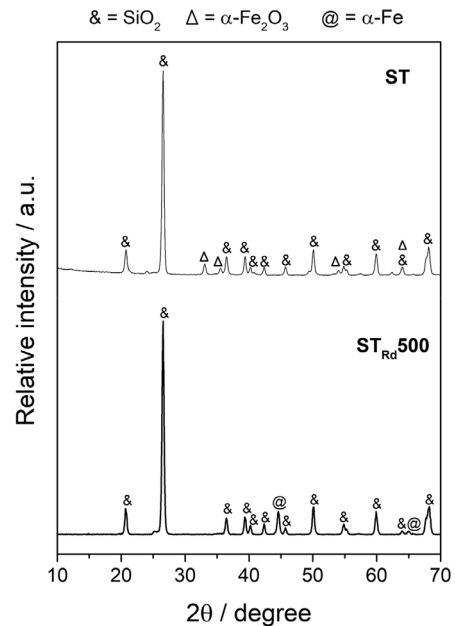
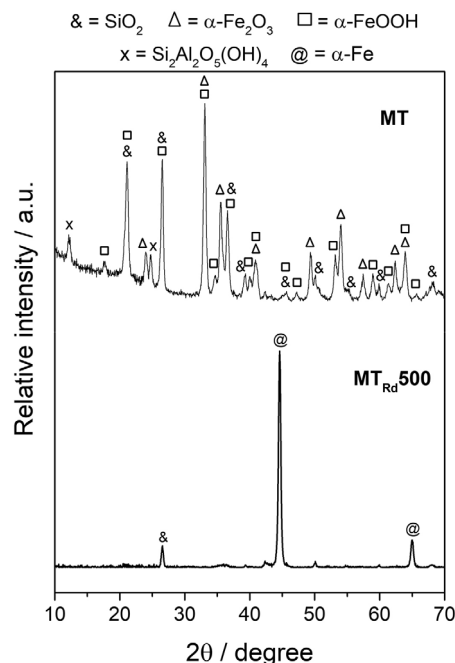
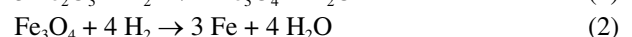
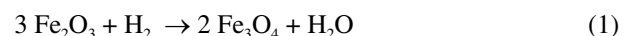
The Raman spectra of ST and MT (Figure 1) showed bands, respectively, at 206, 226, 246, 294, 299, 390, 482, 494, 552, 613, 677 cm⁻¹ and 92, 225, 244, 292, 407, 491, 552, 609, 660 cm⁻¹. They are in agreement with bands related to goethite and hematite³³ for both samples, ST and MT.

**Figure 1.** Raman spectra of ST and MT.

The XRD results (Figure 2) confirmed that the sample ST is composed mainly by silica with a strong peak at 26.6° (JCPDS 46-1045) and very small amounts of crystalline iron oxide as hematite α -Fe₂O₃ (JCPDS 33-664). On the other hand, the sample MT (Figure 3) showed a complex diffractogram pattern with peaks related to SiO₂, α -Fe₂O₃, α -FeOOH (JCPDS 29-713) and the presence of kaolinite, Si₂Al₂O₅(OH)₄ (JCPDS 29-1488).

The IOT samples were directly reduced with hydrogen at 500 °C for 3 h and the phases transformation were analyzed by XRD (Figures 2 and 3). The diffractogram pattern indicated that the iron oxide phases present in the IOT were completely converted to an α -Fe phase (JCPDS 6-696) for both samples.

It is well established that the reduction of α -Fe₂O₃ with hydrogen gas goes through formation of magnetite as a first stage with subsequent formation of metallic iron, as described by equations 1 and 2:³⁴

**Figure 2.** XRD of ST and ST_{Rd}500.**Figure 3.** XRD of MT and MT_{Rd}500.

TPR (temperature programmed reduction) previous data for mud tailing in dynamic mode using 8% H₂ indicated three events centered at 420, 480 and 750 °C. The first two events suggest a reduction of hematite to magnetite, whereas the metal phase α -Fe can only be formed at ca. 750 °C under dynamic conditions.³⁵ Nevertheless, the results presented in this work suggested that the metallic α -Fe can be obtained at 500 °C for 3 h using pure H₂. The reduction of iron oxides in matrices such as tailings is complex and parameters such as H₂ concentration, temperature and reaction time can have a great impact.^{34,36}

The Mössbauer spectra for ST showed the typical sextets for α -FeOOH and α -Fe₂O₃, with a higher spectral area for the latter, of ca. 10 and 90%, respectively (see Figure S1, Table S1, Supplementary Information (SI) section). For the MT sample it is possible to observe three sextets and one doublet. The sextet with greater spectral area (45%) and Mössbauer parameters isomer shift (δ) = 0.35 mm s⁻¹, quadrupole splitting (ΔE_q) = -0.17 mm s⁻¹ and hyperfine field (B_{HF}) = 51.8 T refers to the hematite phase, whereas the sextet with 30% spectral area and δ = 0.38 mm s⁻¹, ΔE_q = -0.28 mm s⁻¹ and B_{HF} = 36.8 T refers to goethite phase (see Figure S1, Table S1, SI section). Additionally, a superparamagnetic phase (sextet), probably related to a highly dispersed Fe³⁺ phase (> 10 nm), and a doublet with a quadrupole splitting of -0.01 mm s⁻¹ related to an aluminosilicate compound in which aluminum was partially substituted by iron were observed.^{37,38}

The Mössbauer spectra of reduced materials (Figure 4) confirmed the results obtained by XRD, whereas the iron oxide phases were converted to an α -Fe phase. However, there was still a small fraction of a Fe³⁺ superparamagnetic phase (6% spectral area) for MT_{Rd}-500, probably related to an internal iron phase that could not be reduced by the hydrogen reduction treatment or an oxidation of metallic iron in the sample at room temperature.

SEM images (Figure 5) of the sample ST showed particles with average sizes between 20-100 μ m mainly related to silica with irregular and rough surfaces. Figueiredo *et al.*³⁹ found similar results for tailings from Fundão dam, after the rupture, collected in Candonga hydroelectric (Brazil). After reduction (Figure 5) no significant change in morphology was observed. The sample MT showed much lower particle sizes, mainly agglomerates of micrometric particles. In this sample, EDS mapping (see Figure S2, SI section) indicated that the silica and Fe oxide are mixed in agglomerated particles.

The EDS mapping of iron and silicon for ST and MT and reduced samples showed that these elements are distributed throughout the samples (see Figures S2 and S3, SI section).

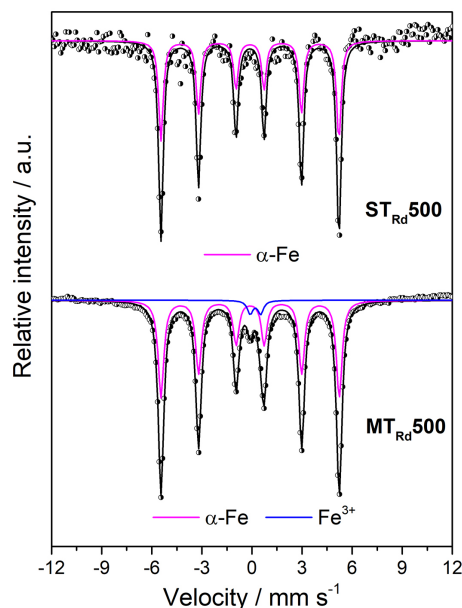


Figure 4. Mössbauer spectra at room temperature of ST_{Rd}500 and MT_{Rd}500.

Magnetic separation

Magnetic separation was carried out with the dry reduced samples using a simple neodymium magnet. Two fractions were obtained, i.e., magnetic fraction (MF) and a non-magnetic fraction (NMF). These fractions were characterized by TG, XRD and SEM, to measure the recovery extension and the chemical composition of each fraction.

After magnetic separation of the sample ST_{Rd}-500 a MF of 15 wt.% and NMF 85 wt.% were obtained whereas for MT_{Rd}-500 most of the sample was magnetic with ca. 77 wt.% MF and 23 wt.% for NMF (Figure 6).

The XRD data for MT_{Rd}500 and its fractions showed that most of MF is composed of α -Fe phase and the MT_{Rd}500_NMF is a mixture of silica and small amounts of α -Fe phases (Figure 7).

The XRD of the NMF of ST_{Rd}500 (Figure 8) showed only the presence of pure silica whereas the MF showed a mixture SiO₂ enriched with α -Fe.

In terms of morphology and composition, SEM images and EDS mapping (Figures 9 and 10) showed clearly Fe enriched MF compared to the silica rich NMF for both samples MT_{Rd}-500 and ST_{Rd}-500 (Figures 9 and 10).

The TG curves for ST_{Rd}-500 showed a weight gain starting at 200 °C, related to α -Fe oxidation to Fe³⁺ oxides of ca. 3.4% (see Figure S4, SI section). As expected, the MF showed a large weight increase of 30% (Figure 11) indicating that most of the Fe was concentrated in the magnetic fraction, corresponding to ca. 87% of Fe enrichment fraction. On the other hand, the NMF did not

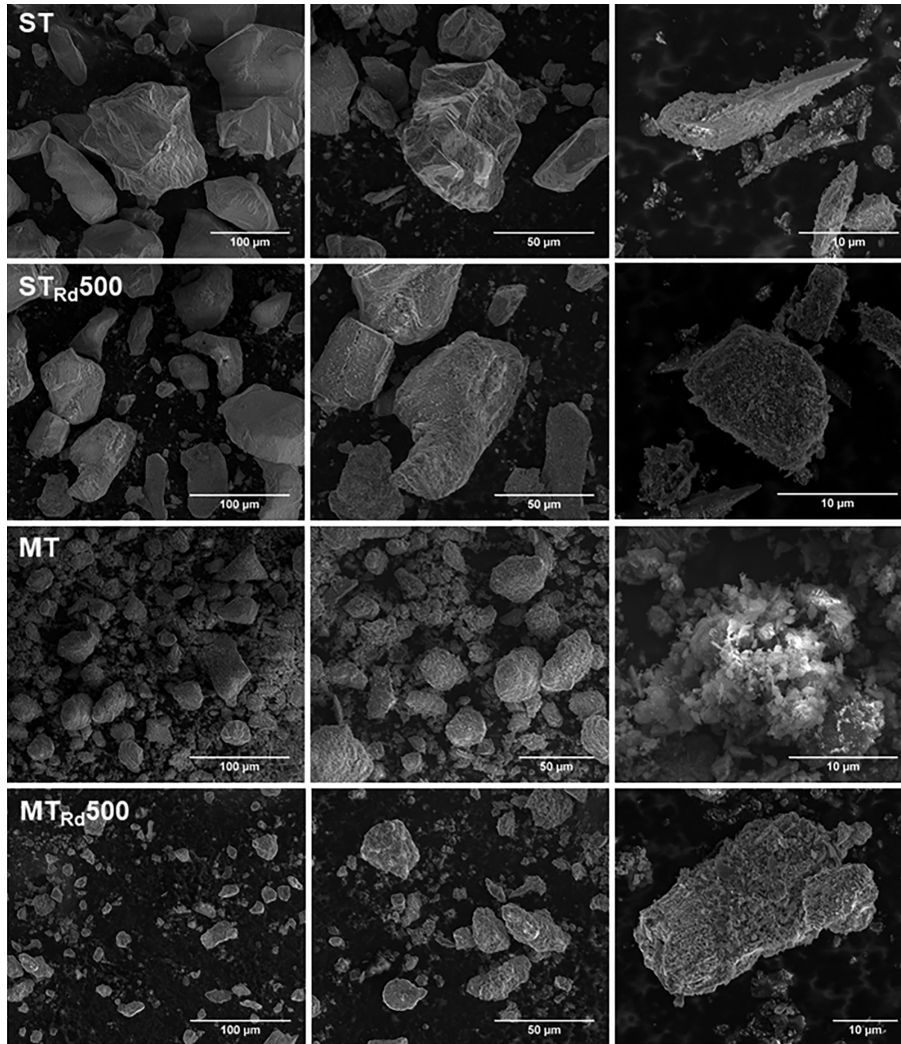


Figure 5. SEM images of ST, ST_{Rd}500, MT and MT_{Rd}500.

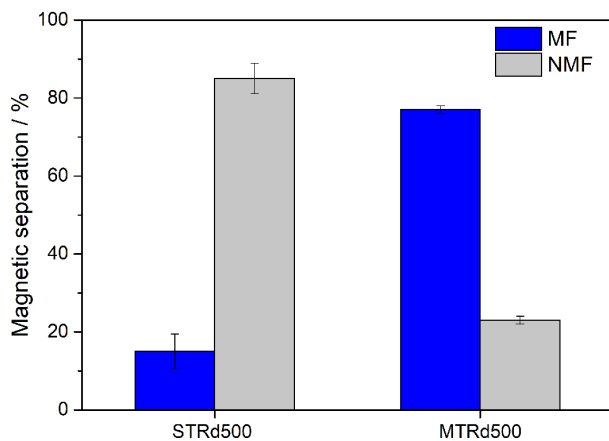


Figure 6. Mass balance after magnetic separation of ST_{Rd}500 and MT_{Rd}500.

show any weight gain indicating that metallic Fe is not significantly present in this fraction (Figure 11).

For the MT_{Rd}500 sample it was observed a weight gain of 22.5% (see Figure S4, SI section). After magnetic

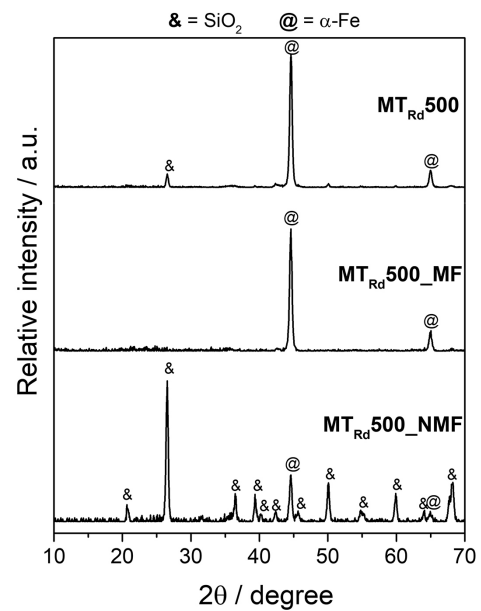


Figure 7. XRD powder diffraction for MT_{Rd}500, MT_{Rd}500_MF and MT_{Rd}500_NMF.

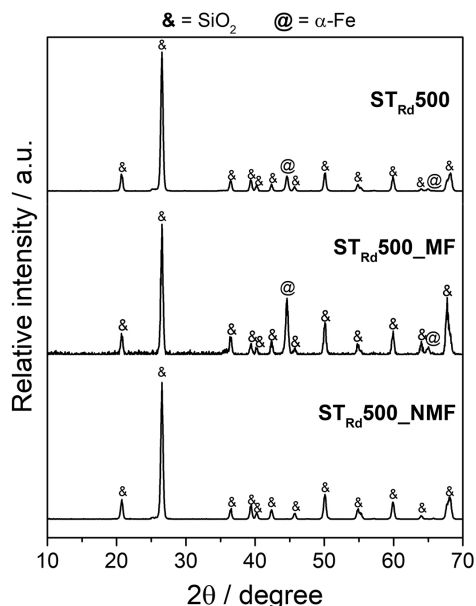


Figure 8. XRD powder diffraction for $ST_{Rd}500$, $ST_{Rd}500_{MF}$ and $ST_{Rd}500_{NMF}$.

separation the NMF showed very small weight gain of ca. 4% whereas the magnetic fraction was ca. 24% indicating a much higher Fe content (Figure 11).

The chemical compositions of reduced IOT's and the magnetic fractions were estimated based on ICP analysis, mass balance, thermal analysis and atomic absorption data (Table 2).

No minimum standards have been set for iron, silica, alumina, calcium, and magnesium percentages in commercial iron ores for steel making. But for commercial viability, the raw iron ores are divided into three classes depending on the total Fe content: (i) high-grade: Fe content above 65%, (ii) medium- or average-grade: Fe contents in the range between 62-64%, and (iii) low-grade: Fe contents below 58%.⁴⁰ In that perspective, the $ST_{Rd}500_{MF}$ is considered a high-grade material that can be used in steel making.

As said before, most works in the literature use greenhouse gases or coke/coal to transform iron oxide from

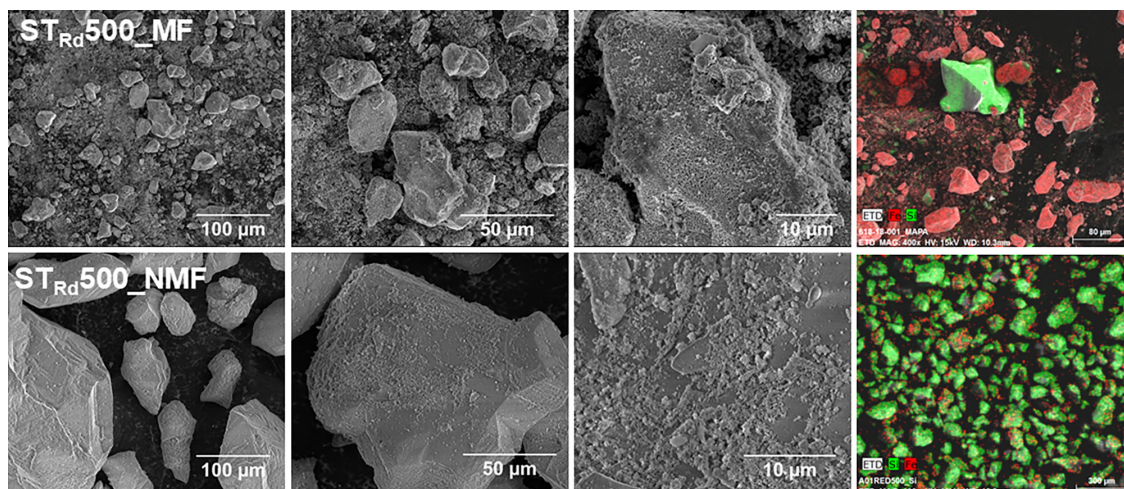


Figure 9. SEM images and EDS mapping of $ST_{Rd}500_{MF}$ and $ST_{Rd}500_{NMF}$.

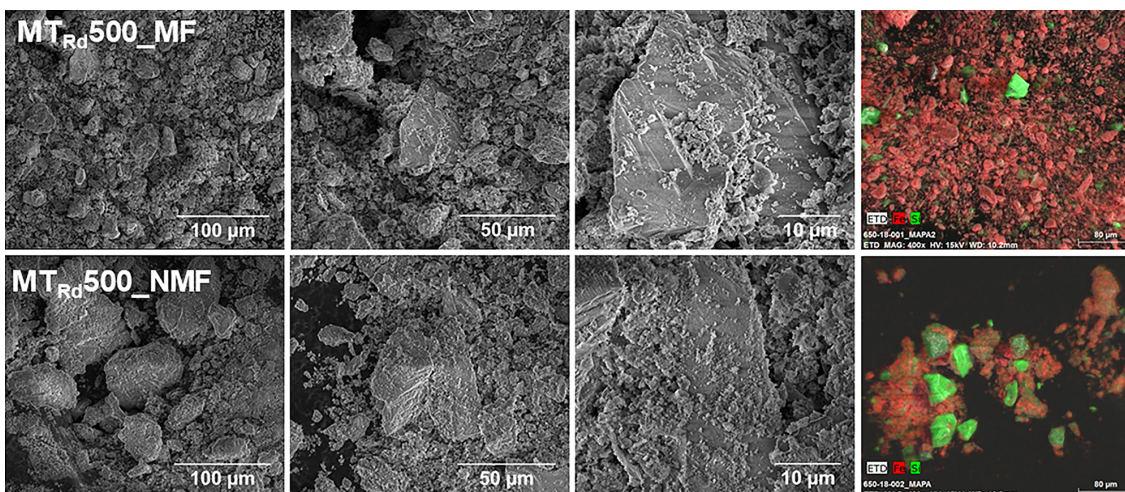


Figure 10. SEM images and EDS mapping of $MT_{Rd}500_{MF}$ and $MT_{Rd}500_{NMF}$.

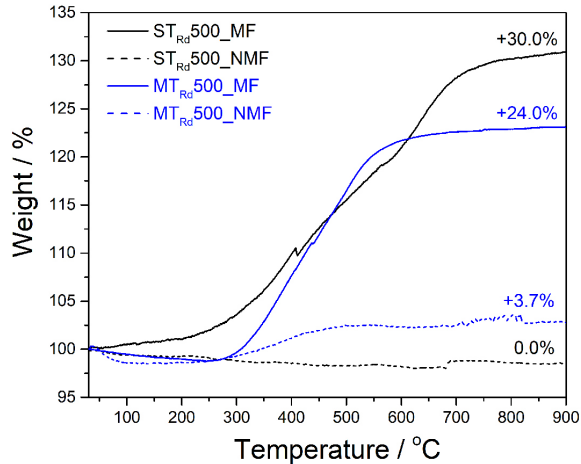


Figure 11. TG analysis, in air atmosphere, for $ST_{Rd}500_MF$, $ST_{Rd}500_NMF$, $MT_{Rd}500_MF$ and $MT_{Rd}500_NMF$.

Table 2. Chemical composition of reduced IOT's and their magnetic fractions in terms of iron and others

Sample	Fe / wt. %	Others / wt. %
$ST_{Rd}500$	20.9	79.1
$ST_{Rd}500_MF$	71.9	28.1
$MT_{Rd}500$	52.7	36.1
$MT_{Rd}500_MF$	56.0	44.0

MF: magnetic fraction; ST: sandy tailing; MT: mud tailing.

iron ore tailings to a magnetic iron phase and subsequently use a magnetic separation for iron recovery. Table 3 shows a comparison of the results obtained in this work and literature. Tang *et al.*⁵ achieved a concentrate assaying 65.91% Fe, in the form of magnetite, with a recovery rate of 94.60% using CO as reducing agent and a roasting temperature of 600 °C. On the other hand, Li *et al.*²⁴ used coal as reducing agent and studied a magnetizing roasting process followed by magnetic separation. The best results achieved a magnetic concentrate of 61.3% Fe and recovery rate of 88.2%, using a ratio of coal:iron ore tailings as 1:100 and roasting at 800 °C. A pre-concentration followed by magnetization roasting and magnetic separation process

Table 3. Comparison of Fe concentrations in tailings initial and after enrichment process in this work and literature

Process/reducing agent	Fe concentration (initial) / wt. %	Fe concentration MF / wt. %	Fe recovery ^a / wt. %	Reference
Direct reduction/ H_2	19.2 ^b	70.0 ^c (71.9) ^d	55	this work (ST)
Direct reduction/ H_2	50.2 ^b	56.0 ^c	86	this work (MT)
Fluidized roasting/CO	10.6	65.9	95	5
Magnetization roasting/coal	11.0	61.3	88	24
Magnetization roasting/CO	10.3	66.4	58	41

^aFe recovery = $\frac{Fe_{\text{final concentration (in the MF)}} \cdot MF_{\text{weight}}}{Fe_{\text{initial concentration (in the IOT)}} \cdot IOT_{\text{weight}}} \times 100$; ^biron concentration as Fe (not as Fe_2O_3) measured by ICP; ^cmeasured by TG weight gain after oxidation;

^dmeasured by atomic absorption. MF: magnetic fraction; ST: sandy tailing; MT: mud tailing.

was used by Zhang *et al.*⁴¹ to obtain a concentrate containing 66.35% Fe with a total recovery of 57.74%. They used a roasting temperature of 540 °C and CO as reducing agent. Besides those works, some researchers also demonstrated the reduction of iron oxides by hydrogen, but no work was found using pure hydrogen and magnetic separation for iron recovery from iron ore tailings.

Our work demonstrated that similar Fe wt.% and recovery rates were obtained with H_2 compared with other processes described in the literature. It was obtained a concentrate containing 70.0% Fe with a total recovery of 55% for $ST_{Rd}500_MF$ and a concentrate containing 56.0% Fe with a total recovery of 86% for $MT_{Rd}500_MF$. As reported by Svoboda and Fujita,⁴² the magnetic separation has some competing forces as the force of gravity, the inertial force, the hydrodynamic drag. In wet separation, the particle size distribution also has a great impact, where the hydrodynamic drag increases, in comparison to the magnetic force, with decreasing of particle size. In this way, the wet magnetic separation used in this work seems to be limited by those parameters. Moreover, it is possible to see in the SEM images that the particles of MT and $MT_{Rd}500$ are mainly composed by aggregations of iron and silica. Then, during the magnetic separation the particles that are attracted to the magnet have both iron and silica phases, which limit the process.

Nevertheless, these results clearly indicate that iron can be enriched by simple direct reduction with hydrogen at relatively low temperatures and subsequent magnetic separation.

Figure 12 shows schematically the process described in this work in terms of iron and its recovery.

Therefore, the process demonstrated in this work is environmental friendly, by using hydrogen, and low cost due to the use of low temperature (500 °C) reduction compared to the literature. Moreover, the magnetic fraction, especially from the ST sample, can be a potential product to the steel industry, since it has a high iron percentage.

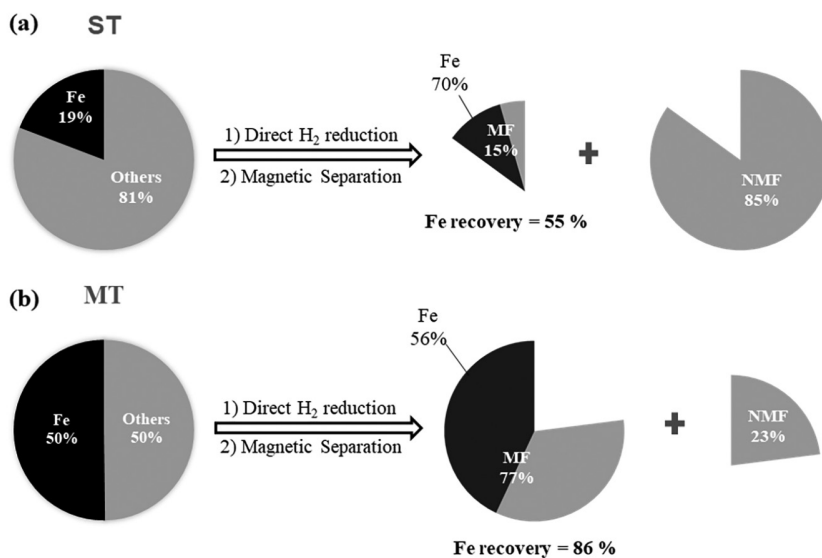


Figure 12. Scheme describing the process in terms of iron and its recovery from (a) ST and (b) MT.

Conclusions

In this work we described a method to convert Fe_2O_3 into $\alpha\text{-Fe}$ and enrich iron from iron ore tailings by direct H_2 reduction at relatively low temperatures and magnetic separation of two types of iron ore tailings with a major composition of iron oxide and silica. The main conclusions were summarized as follows: (i) after direct reduction with H_2 at 500 °C the iron oxide phases were converted to $\alpha\text{-Fe}$ with no significant changes in the particles morphologies; (ii) the magnetic separations demonstrated that the total iron grade for the magnetic fraction was increased from initial 19.2 to ca. 70 wt.% for ST, and from 50 to 56 wt.% for MT. An iron recovery of 55 and 86% Fe was attained under the optimal conditions: using hydrogen gas with a rate flow of 50 mL min^{-1} , a temperature of 500 °C during 3 h.

Supplementary Information

Supplementary data are available free of charge at <http://jbcs.sbq.org.br> as PDF file.

Acknowledgments

The authors gratefully acknowledge the financial support of INCT MIDAS, CNPq, CAPES, FAPEMIG, UFMG Microscopy Center.

Author Contributions

Paula S. Pinto was responsible for conceptualization, data curation, formal analysis, investigation, methodology, validation, visualization,

writing original draft; Luisa E. Milagre for writing original draft; Larissa C. M. Moreira for investigation; Hamilton P. R. Junior for investigation; Adriana B. Salviano for investigation; José D. Ardisson for formal analysis; Ana Paula C. Teixeira for writing review and editing, validation, visualization; Fabrício V. Parreira for funding acquisition; Rochel M. Lago for writing review and editing, conceptualization, funding acquisition, validation, visualization, supervision.

References

1. U.S. Geological Survey; *Mineral Commodity Summaries 2021*; U.S. Geological Survey: Reston, Virginia, 2021, p. 84, available at <https://pubs.usgs.gov/periodicals/mcs2021/mcs2021.pdf>, accessed in March 2022.
2. Zuccheratte, A. C. V.; Freire, C. B.; Lameiras, F. S.; *Constr. Build. Mater.* **2017**, *151*, 859.
3. Sun, Y.; Zhang, X.; Han, Y.; Li, Y.; *Powder Technol.* **2020**, *361*, 571.
4. Darezereshki, E.; Darban, A. k.; Abdollahy, M.; Jamshidi, A.; *J. Alloys Compd.* **2018**, *749*, 336.
5. Tang, Z.; Gao, P.; Li, Y.; Han, Y.; Li, W.; Butt, S.; Zhang, Y.; *Powder Technol.* **2020**, *361*, 591.
6. Carmignano, O. R.; Vieira, S. S.; Teixeira, A. P. C.; Lameiras, F. S.; Brandão, P. R. G.; Lago, R. M.; *J. Braz. Chem. Soc.* **2021**, *32*, 1895.
7. Lima, R. M. F.; Abreu, F. P. V. F.; *J. Mater. Res. Technol.* **2020**, *9*, 2021.
8. Fundação Estadual do Meio Ambiente (FEAM); *Inventário de Resíduos Sólidos da Mineração Ano Base 2017*; FEAM: Belo Horizonte, 2018, p. 47, available at http://www.feam.br/images/stories/2018/RESIDUOS/Inventario_Minera%C3%A7%C3%A3o_ano_base_2017.pdf, accessed in March 2022.

9. Silva Filho, E. B.; Alves, M. C. M.; da Motta, M.; *Matéria (Rio Janeiro)* **2007**, *12*, 322.
10. Segura, F. R.; Nunes, E. A.; Paniz, F. P.; Paulelli, A. C. C.; Rodrigues, G. B.; Braga, G. Ú. L.; dos Reis Pedreira Filho, W.; Barbosa, F.; Cerchiaro, G.; Silva, F. F.; Batista, B. L.; *Environ. Pollut.* **2016**, *218*, 813.
11. Kuranchie, F. A.; Shukla, S. K.; Habibi, D.; Mohyeddin, A.; *Cogent Eng.* **2015**, *2*, 1083137.
12. Huang, X.; Ranade, R.; Ni, W.; Li, V. C.; *Constr. Build. Mater.* **2013**, *44*, 757.
13. Duan, P.; Yan, C.; Zhou, W.; Ren, D.; *Ceram. Int.* **2016**, *42*, 13507.
14. Duan, P.; Yan, C.; Zhou, W.; Ren, D.; *Constr. Build. Mater.* **2016**, *118*, 76.
15. Yang, G.; Deng, Y.; Wang, J.; *Ceram. Int.* **2014**, *40*, 7401.
16. Silva, R. C. F.; Ardisson, J. D.; Cotta, A. A. C.; Araujo, M. H.; Teixeira, A. P. C.; *Environ. Pollut.* **2020**, *260*, 114099.
17. Han, Y.; Zheng, Z.; Yin, C.; Li, P.; Zhang, H.; Hu, Y.; *J. Taiwan Inst. Chem. Eng.* **2016**, *66*, 217.
18. Zheng, J.; Gao, Z.; He, H.; Yang, S.; Sun, C.; *Chemosphere* **2016**, *150*, 40.
19. Teixeira, A. P. C.; Tristão, J. C.; Araujo, M. H.; Oliveira, L. C. A.; Moura, F. C. C.; Ardisson, J. D.; Amorim, C. C.; Lago, R. M.; *J. Braz. Chem. Soc.* **2012**, *23*, 1579.
20. Giri, S. K.; Das, N. N.; Pradhan, G. C.; *Powder Technol.* **2011**, *214*, 513.
21. Praes, P.; Albuquerque, R.; Luz, A.; *J. Miner. Mater. Charact. Eng.* **2013**, *1*, 212.
22. Lima, N. P.; de Souza Pinto, T. C.; Tavares, A. C.; Sweet, J.; *Miner. Eng.* **2016**, *96-97*, 53.
23. Lima, N. P.; Peres, A. E. C.; Gonçalves, T. A. R.; *REM - Int. Eng. J.* **2018**, *71*, 437.
24. Li, C.; Sun, H.; Bai, J.; Li, L.; *J. Hazard. Mater.* **2010**, *174*, 71.
25. Bai, S.-J.; Li, C.-L.; Fu, X.-Y.; Lv, C.; Wen, S.-M.; *Clean Technol. Environ. Policy* **2018**, *20*, 825.
26. Pineau, A.; Kanari, N.; Gaballah, I.; *Thermochim. Acta* **2006**, *447*, 89.
27. Lin, H.-Y.; Chen, Y.-W.; Li, C.; *Thermochim. Acta* **2003**, *400*, 61.
28. Tiernan, M. J.; Barnes, P. A.; Parkes, G. M. B.; *J. Phys. Chem. B* **2001**, *105*, 220.
29. da Costa, A. R.; Wagner, D.; Patisson, F.; *J. Cleaner Prod.* **2013**, *46*, 27.
30. Kazemi, M.; Pour, M. S.; Sichen, D.; *Metall. Mater. Trans. B* **2017**, *48*, 1114.
31. Zuo, H.; Wang, C.; Dong, J.; Jiao, K.; Xu, R.; *Int. J. Miner. Metall. Mater.* **2015**, *22*, 688.
32. Rasband, W. S.; *ImageJ*, 1.52a; U. S. National Institutes of Health, Bethesda, Maryland, USA, 2018.
33. Cornell, R. M.; Schwertmann, U. In *The Iron Oxides*; Wiley-VCH Verlag GmbH & Co. KGaA: Weinheim, 2003, p. 139-183.
34. Sastri, M. V. C.; Viswanath, R. P.; Viswanathan, B.; *Int. J. Hydrogen Energy* **1982**, *7*, 951.
35. da Cunha, J. B. V.; *Obtenção e Caracterização de Fotocatalisadores Heterogêneos a Partir de Rejeito da Mineração de Ferro e sua Aplicação na Remoção de Contaminantes Emergentes*; MSc Dissertation, Universidade Federal de Minas Gerais, Belo Horizonte, 2018, available at <https://repositorio.ufmg.br/handle/1843/SFSA-B4LPQG>, accessed in March 2022.
36. Cornell, R. M.; Schwertmann, U. In *The Iron Oxides*; Wiley-VCH Verlag GmbH & Co. KGaA: Weinheim, 2003, p. 365-407.
37. Hogg, C. S.; Meads, R. E.; *Mineral. Mag.* **1970**, *37*, 606.
38. Murad, E.; *Clay Miner.* **2010**, *45*, 413.
39. Figueiredo, M. D.; Lameiras, F. S.; Ardisson, J. D.; Araujo, M. H.; Teixeira, A. P. C.; *Integr. Environ. Assess. Manage.* **2020**, *16*, 636.
40. Muwanguzi, A. J. B.; Karasev, A. V.; Byaruhanga, J. K.; Jönsson, P. G.; *ISRN Mater. Sci.* **2012**, *2012*, 174803.
41. Zhang, X.; Han, Y.; Sun, Y.; Lv, Y.; Li, Y.; Tang, Z.; *Miner. Process. Extr. Metall. Rev.* **2020**, *41*, 117.
42. Svoboda, J.; Fujita, T.; *Miner. Eng.* **2003**, *16*, 785.

Submitted: October 30, 2021

Published online: March 24, 2022

